Optimization of light scattering enhancement by gold nanoparticles in fused silica optical fiber

Wang, Xiang; Benedictus, Rinze; Groves, Roger M.

DOI
10.1364/OE.427967

Publication date
2021

Document Version
Final published version

Published in
Optics Express

Research Article | Vol. 29, No. 13 / 21 June 2021 / Optics Express 19450
Optics EXPRESS

Optimization of light scattering enhancement by gold nanoparticles in fused silica optical fiber

XIANG WANG,* RINZE BENEDICTUS, AND ROGER M. GROVES

Faculty of Aerospace Engineering, Delft University of Technology, 2629 HS Delft, The Netherlands
Xiang.Wang@tudelft.nl

Abstract: A conventional distributed fiber optic sensing system offers close to linear sensitivity along the fiber length. However gold nanoparticles (NP) have been shown to be able to enhance the contrast ratio to improve the quality of signal detection. The challenge in improving the contrast of reflected signals is to optimise the nanoparticle doping concentration over the densed sensing length to make best use of the distributed fiber sensing hardware. In this paper, light enhancement by spherical gold NPs in the optical fibers was analyzed by considering the size-induced NP refractive index changes. This was achieved by building a new model to relate backscattered light from a gold NP suspension between the optical fiber end tips and backscattered light from gold NPs in the core of the optical fiber. The paper provides a model to determine the optimized sizes and concentrations of NPs for sensing at different desired penetration depths in the optical fiber.

1. Introduction

Backscatter reflectometry uses the refractive index (RI) variation of the optical distribution features along the sensing fiber to sense parameters such as strain and temperature [1]. It has been widely used for structural health monitoring (SHM) in aerospace engineering [2–4] and civil engineering [5]. As the sensor used to sense these parameters depends on the backscattered light intensity, a low intensity scattering signal from the intrinsic RI fluctuation of the optical fiber is one of the limitations of this technique.

One approach to solve this problem is to dope nanoparticles (NP) into the core of the optical fiber to increase the scattered light signals in the backscatter reflectormetry. Blanc and Dussardier [6] described the methods of manufacturing NP-doped in silica optical fiber and analyzed the optical intensity loss with Rayleigh scattering. Later Molardi et al. [7] investigated the characteristics of MgO-doped optical fiber and obtained a 50 dB scatterred light increase experimentally. They pointed out the potential use of this approach for spatial multiplexing in optical backscatter reflectometry. Beisenova et al. [8] presented experimental results of 3D shape sensing with a MgO doped optical fiber in a spatial multiplexing structure for an epidural needle. Bulot et al. [9] improved the stability of temperature sensing at a high temperature with zirconia-coated gold NP doped optical fiber in optical frequency domain reflectometry (OFDR) distributed sensing. These works show the feasibility and the advantages of doping NPs into the core of the optical fibers for distributed sensing, but do not address the optimization of the NP concentration.

We chose gold NPs to be doped into the optical fiber to increase the scattered signals. As a commonly used NP, gold NP has previously been investigated to increase the image contrast for optical coherence tomography (OCT) detection, for example as a bio-compatible contrast agent in tissue [10–13]. The reason for choosing gold NPs is that gold NPs have a relatively high reflection coefficient compared to other materials with the same diameter. This is also shown in Fig. 1, where it can be seen that gold NPs in particular have relatively high scattering efficiencies compared to other metals in fused silica. Another reason is that gold is relatively stable and hard to oxidise. Figure 1 also shows that metal oxides in general have lower scattering efficiencies than

#427967 https://doi.org/10.1364/OE.427967
Journal © 2021 Received 15 Apr 2021; revised 7 May 2021; accepted 13 May 2021; published 8 Jun 2021

Optics EXPRESS

metals. Therefore, optical fiber doped with gold might have the potential to be used as highly scattering fiber optic sensors.

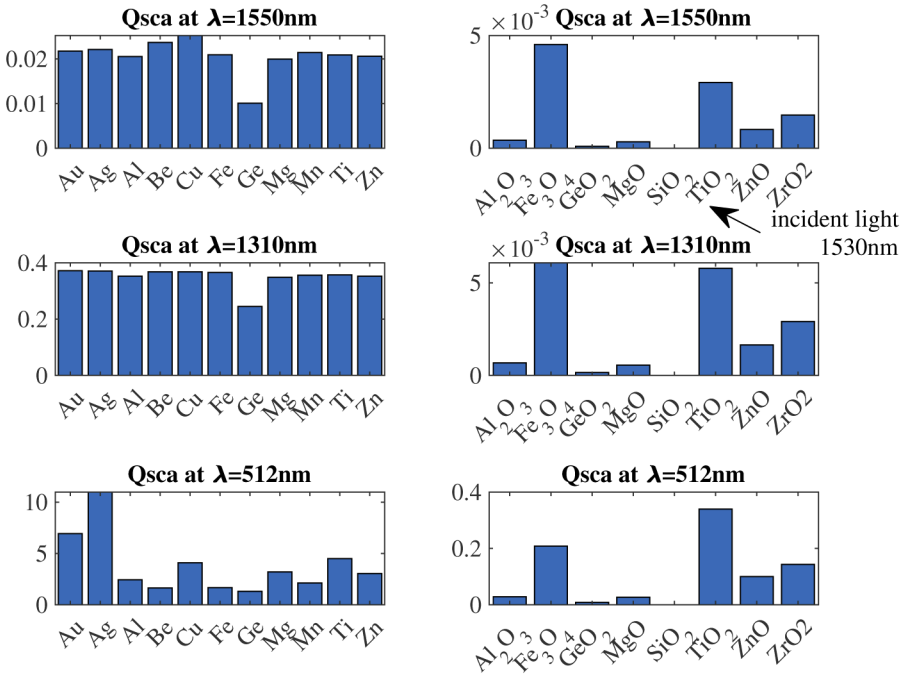

Fig. 1. The scattering efficiencies for small particles (100 nm diameter) of a variety of materials. The scattering efficiencies were calculated by Mie theory for small particles compared with the wavelengths.

The specific scattering characteristics of gold NPs in optical fiber have not been previously investigated, so the optimized sizes and concentrations of NPs to be doped in the optical fiber to increase the scattered light is unclear.

In our previous work [14], we investigated a method of dropping liquid containing gold NPs at optical fiber end tips to obtain the backscattered light by the gold NPs at the interfaces. We evaluated the levels of light scattering by gold spherical NPs by modelling a broadband light source whose central wavelength was around 1550 nm. The experimental results from our previous work [14] showed that it is a challenge to detect the scattered light from NPs by means of direct light intensity detection, although the highly sensitive detection method, OCT [15] is a suitable choice. Some OCT systems have the ability to achieve a high sensitivity over100 dB [16].

In this work, a novel model connecting size and concentration of gold NP in the core of the optical fiber with the backscattered light signals by a gold NP suspension between the optical fiber end tips to the backscattered light signals will be built. By obtaining the relationship between backscattered light signals at optical fiber end tips, the equivalent backscattered light by NPs in the optical fiber can be obtained. We are then able to determine the optimized intensity of scattered light from NPs within the desired penetration depths in the optical fiber. An OCT system [17] will be used to detect the scattered light signals from the gold NP suspension between the optical fiber end tips.

This paper is organized in four sections. The first section is the introduction. The model for analyzing the optimized scattered light with an OCT is described in Section 2. The results and discussion for different size NPs (1 nm to 400 nm) under a wide wavelength range (400 nm to 1600 nm) are presented in Section 3. Section 4 is the conclusion.

Optics EXPRESS

2. Model

An optical fiber containing gold NPs in the core is shown schematically in Fig. 2(a). The gold NPs are assumed to be homogeneous spherical NPs, which are well dispersed in the core of the optical fiber with a constant concentration. The incident light propagates along the core of the optical fiber from the left side to the right side and the light is scattered by the NPs. The scattered light in the backward direction within the total internal reflection angle in the core of the optical fiber is considered reflected. In this work, we are interested in increasing the backscattered light by NPs within a desired NP-doped optical fiber sensor's length to maximize the intensity of backscattered light distributed along an optical fiber for Structural Health Monitoring applications.

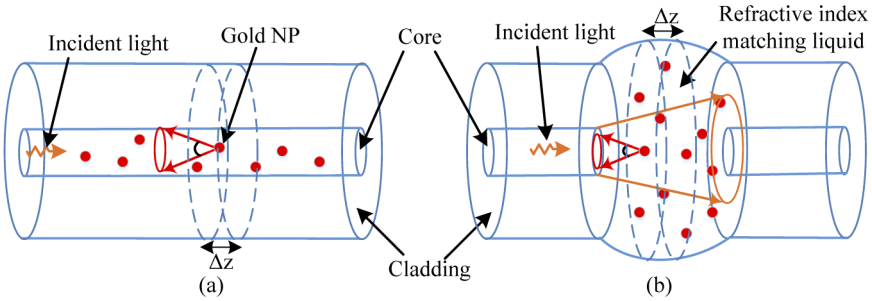

Fig. 2. Models of scattered light from NPs. (a) Light scattered by the gold NPs in the core of optical fiber; the red dots represent the gold NPs with a constant concentration; propagating light is in orange and the backscattered light is in red with directions; Δz is the spatial resolution for the regions containing gold NPs. (b) Light scattered by the gold NPs at optical fiber interfaces.

Figure 2(b) shows the structure of the optical fiber end tips. Refractive index (RI) matching liquid containing gold NPs has been dropped at the interfaces. The optical fiber interfaces model is more flexible for laboratory experimental work [14] and will be used here to determine the optimized concentrations of NPs. To obtain the high sensitivity of the backscattered light detection, an OCT system is used which is shown in Fig. 3. As shown in Fig. 3, incident light is

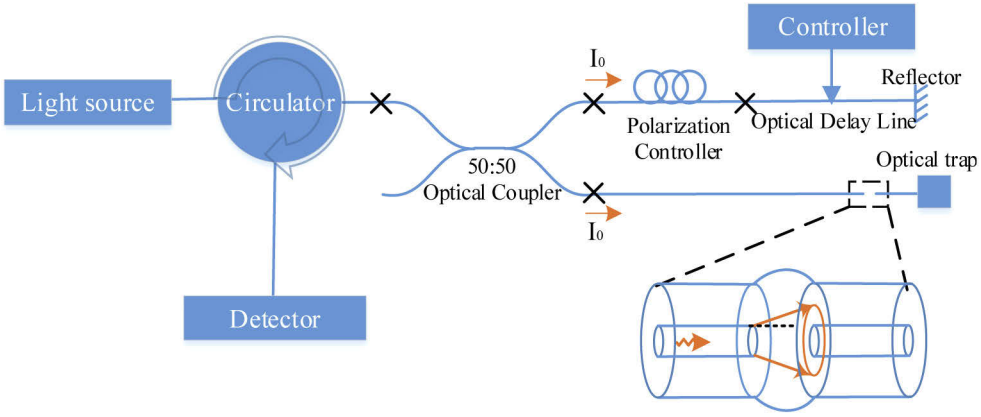

Fig. 3. The basic structure of the optical detection system combined with OCT to realize the detection of the scattered light from the NPs between the optical fiber interfaces. The optical fiber interface part has been enlarged for clarity. The mounting system for the optical fiber end tips is not shown.

Optics EXPRESS

emitted from a broadband light source and then propagates into an optical coupler via an optical circulator. The light is split into two beams with a split ratio 50:50. One of the beams (light power I_0) propagates in the reference arm and is then reflected by a reflector. The other beam (light power I_0) propagates in the sample arm and is scattered by the NPs at the optical fiber end tips. By changing the distance of the reference arm by the optical fiber delay line and tuning the polarization of the light by the polarization controller, the reflected light in the reference arm will interfere with the scattered light by the NPs in the sample arm. The interference signals will be measured by the detector.

By constituting the relationship between the backward scattered light in the liquid and the equivalent light scattered by NPs in the core of optical fiber, the latter can be determined.

In the following sections, we will recall the model of light scattering by NPs at optical fiber interfaces and then compare it with the model of light scattering by NPs in the core of optical fiber to build the relationship between these two models. Once the relationship is obtained, we can derive the case of scattered light by the NPs in the optical fibers by making use of the NP optical fiber end tip interface model.

2.1. Light scattering at optical fiber interfaces

In our previous work [14] we analyzed the scattered light at optical fiber interfaces as shown in Fig. 2(b). The expression of the recoupled scattered light, I_{recouple}, by the gold NPs is

$$I_{\text{recouple}} = \int_V cT_1 \left(\int_\lambda I_{\text{wavelength}}(x, y, z, \lambda) I'_s(\lambda) \exp(-\alpha z)\, \mathrm{d}\lambda \right) \mathrm{d}V, \tag{1}$$

where V is the liquid volume within a certain spatial interval Δz; c is the concentration of gold NPs in RI matching liquid; T_1 is the transmittance between the optical fiber end tip and the liquid; λ is the wavelength of the incident light; $I_{\text{wavelength}}$ is the spatial intensity distribution of the light incident on the NPs; x, y, and z are the spatial positions of the centre of the NPs; I'_s is the scattering response by NPs which can be recoupled into the left optical fiber and α is the attenuation caused by the absorption from RI matching liquid and the extinction by NPs.

In Eq. (1), the single scattering model is used due to the concentration of NPs (optical depth $\tau = cC_{\text{ext}}z<1$[18]), where C_{ext} is the extinction cross section of the NP. The light backscattered by the NPs propagates backwards and attenuates by absorption in the RI matching liquid and extinction by the NPs. Then, the backscattered light is recoupled into the optical fiber.

Due to the relatively small sizes of NPs (1 nm to 400 nm) in the RI matching liquid, the propagating light incident on the NPs is regarded as a plane wave which can be treated with Mie theory [19].

The spatial intensity distribution of the light in the liquid was modelled as Gaussian-profile planes with a z-distance-related profile amplification ratio. The spectra of the incident light was modelled as a Gaussian distribution spectra (see [14] for further details).

If we use the scattering intensity $|\chi|^2$ of the NP in the backward direction as the mean scattering intensity, I'_s, can be approximated as

$$I'_s(\lambda) \approx \frac{(\lambda/n_{\text{liquid}})^2}{\pi} |\chi(\pi)|^2 \gamma(x, y, z) \frac{\Omega}{4\pi}, \tag{2}$$

$$\Omega = 2\pi(1 - \cos\zeta), \tag{3}$$

where n_{liquid} is the RI of the RI matching liquid; $\gamma(x, y, z)$ is the coupling efficiency of the light scattered by NPs at positions (x, y, z); and ζ is the numerical aperture angle in the liquid. Note: the values of $\chi(\pi)$ are related to the incident light wavelengths. For a broadband light source, if $\chi(\pi)$ and the RI of the medium can be regarded as constants for a certain size spherical gold NPs

Optics EXPRESS

and the spatial interval is small, then Eq. (1) can be approximated as

$$I_{\text{recouple}} = BI_0C(z)\Delta z\mu_b\Omega\exp(-2\alpha z_0), \tag{4}$$

where

$$B = \frac{T_1^2}{8\pi^2}, \tag{5}$$

$$C(z) = \frac{2\pi}{(2\sigma_0/k(z_0))^2\,\pi/2}\int_0^\infty \exp\left(-2\left(\frac{r}{2\sigma_0/k(z_0)}\right)^2\right)\gamma r\,\mathrm{d}r, \tag{6}$$

where $\Delta\lambda$ is the full width at half maximum (FMHW) of the light source, λ_c is the central wavelength of the light source, z_0 is the centre of the spatial interval, k is the profile amplification ratio, $r = \sqrt{x^2+y^2+z^2}$ and $2\sigma_0$ represents the mode field radius of the incident light in the optical fiber.

The form of Eq. (4) is similar to the case of a OCT system with the light focused in the sample path [20,21], but adjusted by $B(z)$ according to the bandwidth of the light source. The aperture function [22,23] of the interferometer from a focus lens has been substituted by $C(z)$ for the case of interfaces.

2.2. Light scattering in the core of optical fiber

Under the same assumptions, the backscattered light by the NPs in the optical fiber can be expressed as

$$I'_{\text{recouple}} = \int_V c\left(\int_\lambda I'_{\text{wavelength}}(x,y,z,\lambda)I''_s(\lambda)\exp(-\alpha' z)\,\mathrm{d}\lambda\right)\mathrm{d}V, \tag{7}$$

where $I'_{\text{wavelength}}$ is the light propagating in the optical fiber; and I''_s is the scattered light by the NPs which propagates backwards in the optical fiber. As the light is confined in the optical fiber, the expression for the light propagating in the optical fiber can be expressed as

$$I'_{\text{wavelength}}(x,y,z,\lambda) = \exp(-\alpha' z)\times I(\lambda)\times\frac{1}{(2\sigma_0))^2\,\pi/2}\times\exp\left(-2\left(\frac{r}{2\sigma_0}\right)^2\right). \tag{8}$$

$I''_s(\lambda)$ has the same form as Eq. (2).

$$I''_s(\theta',\varphi',r',\lambda) \approx \frac{(\lambda/n_{\text{liquid}})^2}{\pi}|\chi(\pi)|^2\Gamma\frac{\Omega'}{4\pi}. \tag{9}$$

$$\Omega' = 2\pi(1-\cos\zeta') \tag{10}$$

where Γ is the coupling efficiency in the optical fiber, and ζ' is the numerical aperture angle in the core of the optical fiber.

In this case, the light scattered by the NPs at the z_0 position with spatial resolution Δz propagates backwards along the fiber and can be expressed as

$$I'_{\text{recouple}} = B'I_0C'(z)\Delta z\mu_b\Omega'\exp(-2\alpha' z_0). \tag{11}$$

where

$$B' = \frac{1}{8\pi^2}, \tag{12}$$

$$C'(z) = \Gamma \tag{13}$$

α' is the attenuation coefficient caused by the absorption by the optical fiber and the extinction by the NPs.

Optics EXPRESS

Comparing Eqs. (4) and (11), the relationship between the two models can be obtained

$$I'_{\text{recouple}} = I_{\text{recouple}} \times \frac{1}{T_1^2} \times \frac{\Gamma}{C(z)} \times \frac{\Omega'}{\Omega} \times \exp(-2(\alpha' - \alpha)z_0). \tag{14}$$

According to Eq. (14), when the light is recoupled into the liquid (I_{recouple}), the transmittance of the interfaces between liquid and fiber (T_1), the spatial coupling efficiency in the liquid ($C(z)$), the coupling efficiency in the core of optical fiber (Γ), and Ω', Ω, α' and α are given or can be obtained from experiments or simulations. Therefore the equivalent backscattered light in the optical fiber can be calculated.

2.3. Signal detection by OCT and the light enhancement evaluation

For an OCT system, if the optical coupler split ratio is 50:50, the signal detected by the photodetector can be expressed as [20,24]

$$i(z) = KI_0\sqrt{BC(z)L_c}\sqrt{\mu_b\Omega}\exp(-\alpha z), \tag{15}$$

where K is the gain of the photodetector and I_0 is the light power in the sample arm to incident on the gold NPs (Note: in this case the total light power from the light source is $2I_0$). For light that is in the core of optical fiber, as shown in Fig. 2(a), the signal detected by the photodetector can be expressed as

$$i'(z) = KI_0\sqrt{B'C'(z)L_c}\sqrt{\mu_b\Omega'}\exp(-\alpha' z), \tag{16}$$

where I_0 is also the light power incident on the gold NPs.

Therefore, the relationship between the signal detected by the core of optical fiber $i'(z)$ and that detected in liquid $i(z)$ can be expressed as

$$i'(z) = i(z) \times \sqrt{\frac{1}{T_1^2} \times \frac{\Gamma}{C(z)} \times \frac{\Omega'}{\Omega}} \times \exp(-(\alpha' - \alpha)z_0). \tag{17}$$

According to the form of Eqs. (15) and (16), we define the light enhancement coefficient $R_{\text{enhancement}}$ from the NPs for both cases as

$$R_{\text{enhancement}}(z) = \sqrt{\mu_b}\exp(-\mu_t z). \tag{18}$$

We will use Eq. (18) to show the system response to scattered light by the NPs at z positions, $\mu_t = \alpha'$ for the case in the RI matching liquid and $\mu_t = \alpha$ for the case in the core of optical fiber.

As shown in Eq. (18), the enhancement is caused by the backscattering from NPs (μ_b), but the light loss is adjusted by μ_t. $\mu_t = \mu_{\text{extNP}} + \mu_{\text{aMedium}}$ where μ_{extNP} is the light extinction caused by NPs and μ_{aMedium} is the absorption by the media.

We define the depth of the detected signal with 3dB loss as the penetration depth, which also means the light enhancement coefficient $R_{\text{enhancement}}$ loses half of its value at depth $z = l_{\text{depth}}$. This part of the loss is the light extinction by introducing the NPs (Note: the total loss is the combination of both the loss caused by the NPs and the loss caused by the medium). Then, the penetration depth seen by the detector can be expressed as

$$l_{\text{depth}} = \frac{\ln 2}{\mu_{\text{extNP}}}. \tag{19}$$

A high enhancement within an expected penetration depth is expected. More details about the relevant parameters of the light enhancement coefficient in Eq. (18) (μ_b and μ_t) will be described in the next part.

Optics EXPRESS

2.4. Parameters used for light enhancement by gold NPs

When the concentration of the NPs is low only single scattering from the NPs is considered. In this case, $\mu_{\text{extNP}} = cC_{\text{ext}}$[19], where c is the concentration namely the number of particles in a unit volume and C_{ext} is the extinction cross section of the NP. In this paper, we consider monotonous spherical particles, so $\mu_{\text{extNP}} = cC_{\text{ext}} = c\pi(D/2)^2 Q_{\text{ext}}$, where D is the diameter of the NP, $\mu_b = c\pi(D/2)^2 Q_b$, $Q_{\text{ext}t}$ is the extinction coefficient and Q_b is the backscattering coefficient of a NP. If we assume the volume ratio (ρ) of the NPs to the liquid to be

$$\rho = \frac{V_{NPs}}{V_{liquid}} = c\frac{4\pi}{3}\left(\frac{D}{2}\right)^3, \tag{20}$$

then $\sqrt{\mu_b}$ and μ_{extNP} can be expressed as

$$\sqrt{\mu_b} = \sqrt{\rho\frac{3}{2D}Q_b}, \tag{21}$$

$$\mu_{\text{extNP}} = \rho\frac{3}{2D}Q_{\text{ext}}. \tag{22}$$

Q_b is the scattering intensity enhancement from the NPs and Q_{extNP} is the signal attenuation through the depth, caused by the NPs. Therefore, the penetration depth can be expressed as

$$l_{\text{depth}} = \frac{2D\ln 2}{\rho 3 Q_{\text{ext}}}. \tag{23}$$

Therefore, if the scattering parameters (for example, Q_{ext}, Q_b) are obtained the enhancement of the scattered light is determined.

Mie theory [19] was used to illustrate the influence of different sizes of gold NPs at different incident wavelengths. Scattering efficiency and extinction efficiency were taken into comparison for these cases to show the ratio of light scattered by the gold NPs to the extinction ratio.

The definition of scattering efficiency is [19]

$$Q_{\text{sca}} = \frac{2}{x^2}\sum_{n=1}^{\infty}(2n+1)\left(|a_n|^2 + |b_n|^2\right) \tag{24}$$

The definition of extinction efficiency is

$$Q_{\text{ext}} = \frac{2}{x^2}\sum_{n=1}^{\infty}(2n+1)\,\text{Re}\,(a_n + b_n) \tag{25}$$

The absorption efficiency can then be calculated as

$$Q_{\text{abs}} = Q_{\text{ext}} - Q_{\text{sca}} \tag{26}$$

where x is the size parameter, a_n and b_n are the scattering coefficients in the Mie calculation [19] and Q_b is the backscattering efficiency, which is defined as [19]

$$Q_b = \frac{1}{x^2}\left|\sum_{n=1}^{\infty}(2n+1)(-1)^n(a_n - b_n)\right|^2 \tag{27}$$

The size parameter x is related to the ratio of the RI of the particle to the medium. Generally, the RI of bulk gold can be used in the calculation when the size of the particle is large. However, for small size gold particles especially the nanometer size gold particles in this paper, the refractive

Optics EXPRESS

indices at smaller sizes will have an influence on the scattering and extinction efficiencies. Therefore, the size-induced RI change of gold NPs needs to be considered.

The specific size-dependent complex dielectric function of gold NPs can be expressed as [25]

$$\epsilon(\omega) = 1 - \frac{\omega_p^2}{\omega^2 + i(\gamma_{\text{bulk}+H\frac{\nu_F}{R}})\omega} + Q_{\text{bulk}}[1 - \exp(-\frac{R}{R_0})]G(\omega), \tag{28}$$

$$G(\omega) = \int_{\omega_g}^{\infty} \frac{\sqrt{\omega' - \omega_g}}{\omega'}[1 - F(\omega', T)]\frac{\omega'^2 - \omega_g^2 + \gamma_b^2 + i2\omega\gamma_b}{(\omega'^2 - \omega_g^2 + \gamma_b^2)^2 + 4\omega^2\gamma_b^2}\,\mathrm{d}\omega', \tag{29}$$

where ω and ω' are the angular frequency, ω_p is the bulk plasma frequency of gold, γ_{bulk} is the damping constant for free electrons, H is a scattering constant, ν_F is the electron velocity at the Fermi surface, R is the radius of the gold particle, Q_{bulk} is the coefficient for bound electron contribution, R_0 is the fit value, ω_g is the frequency corresponding to the gap energy of gold, $F(\omega, T) = 1/(\exp\frac{\hbar\omega - E_f}{k_b T} + 1)$ is the Fermi energy distribution, k_b is the Boltzmann constant, E_f is the Fermi energy and γ_b is the damping constant for bound electrons. The specific values of these parameters used are shown in Table 1.

Table 1. Relevant Parameters for Calculating the Complex Dielectric of Gold

Parameter	Value
ω_p	13×10^{15} Hz [26]
γ_{bulk}	1.1×10^{14} Hz [27]
H	0.8 [25]
ν_F	14.1×10^{14} nm s^{-1} [26]
Q_{bulk}	2.3×10^{24} [25]
R_0	0.35 nm [25]
ω_g	3.19×10^{15} Hz [25]
E_f	2.5 eV [25]
T	301.5 K
γ_b	2.4×10^{14} Hz [28]

The calculated results of RI within the 400 nm to 1600 nm incident light range match the experimental data [27] when $R = \infty$ in Eq. (28). Therefore, the RI calculation matches the experimental data well between 400 nm to 1600 nm for bulk gold. When the sizes of the gold NPs are small, the values of RI will deviate from the experimental data from bulk gold. We define this deviation (error), to evaluate the influence of size-induced scattering parameters changes, with the expression

$$\text{Error}Q_i = \frac{Q_{i-\text{nano}} - Q_{i-\text{bulk}}}{Q_{i-\text{nano}}} \times 100\%, \quad i = b, \text{sca}, \text{abs}, \text{ext}, \tag{30}$$

where b, sca, abs, and ext represent backward scattering, scattering, absorption and extinction respectively.

When the RI of bulk gold is used in the calculation for the gold NPs in fused silica, errors will arise. To evaluate these errors, Eq. (30) is used. Figure 4(a) shows the errors between backscattering efficiencies calculated using the RI of gold NPs and the RI of bulk gold. The RI of the medium (fused silica) used is from Malitson's work [29]. Very high errors occur when the diameters of the NPs are less than 10 nm and when the wavelength is around 500 nm. If the backscattering efficiency needed is in this range, the size-induced refractive index change should be treated carefully. When the size of the NPs and the wavelengths deviate from this

Optics EXPRESS

region, the errors are relative small (below 10 %). The errors in the extinction efficiencies are shown in Fig. 4(b). Figure 4(c) shows the errors for the absorption efficiencies. The similarity of Figs. 4(b) and 4(c) shows that the errors in absorption efficiencies are the main influence on the errors in extinction efficiencies and scattering and the errors in backscattering have a relatively low influence on the extinction parameter errors.

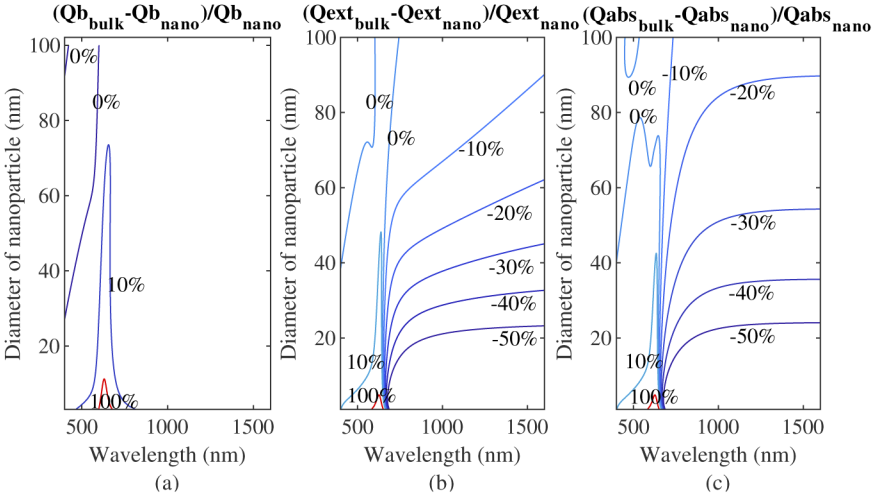

Fig. 4. Calculated scattering parameters errors between size-dependent refractive index and bulk refractive index, the wavelength range is from 400 nm to 1600 nm, the diameter range of NPs is from 1 nm to 100 nm. (a) The backscattering efficiency errors. (b) The extinction efficiency errors. (c) The absorption efficiency errors in fused silica.

From the analyses above, it can be seen that in most of the region the size-induced efficiency changes are small, but for a more precise calculation, in this paper we will use the size-dependent RI for gold NPs.

The attenuation of the medium (fused silica) can be expressed as [30,31].

$$\mu_{\text{aMedium}} \approx \alpha_{\text{Rayleigh}} + \alpha_{\text{IR}} \tag{31}$$

where α_{Rayleigh} is the loss caused by the density density fluctuations of the material and α_{IR} is the loss caused by the vibration absorption in fused silica.

$$\alpha_{\text{Rayleigh}} = 5 \times 10^{-5} n_0^2 p^2 K_T(T_g) T_g / \lambda^4 \tag{32}$$

where $n_0 = 1.46$; $p = 0.22$; $K_T \approx 6 \times 10^{-11}$/Pa in units of 10^{-11}/Pa in Eq. (32), $T_g = 1450K$, λ in unit μm [30].

$$\alpha_{\text{IR}} = A_i \exp(-a_i/\lambda) \tag{33}$$

where $A_i \approx 6 \times 10^{11}$ dB/km and $a_i \approx 48$ μm [30].

3. Results and discussion

3.1. Scattering characteristics for same volume ratios gold NPs in fused silica

Figure 5 shows the scattering character from homogeneous NPs with a certain concentration in the same volume ratio. The values of $\sqrt{\mu_b}/\sqrt{\rho}$ are shown in Fig. 5(a). $\sqrt{\mu_b}$ equals the light enhancement coefficient at $z = 0$ ($R_{\text{enhancement}}(0)$).

It is well-known that the intensities and the angles of the scattering lobes depend on ratio of the size of the NPs and the wavelength of the incident light and the refractive index. A larger size

Optics EXPRESS

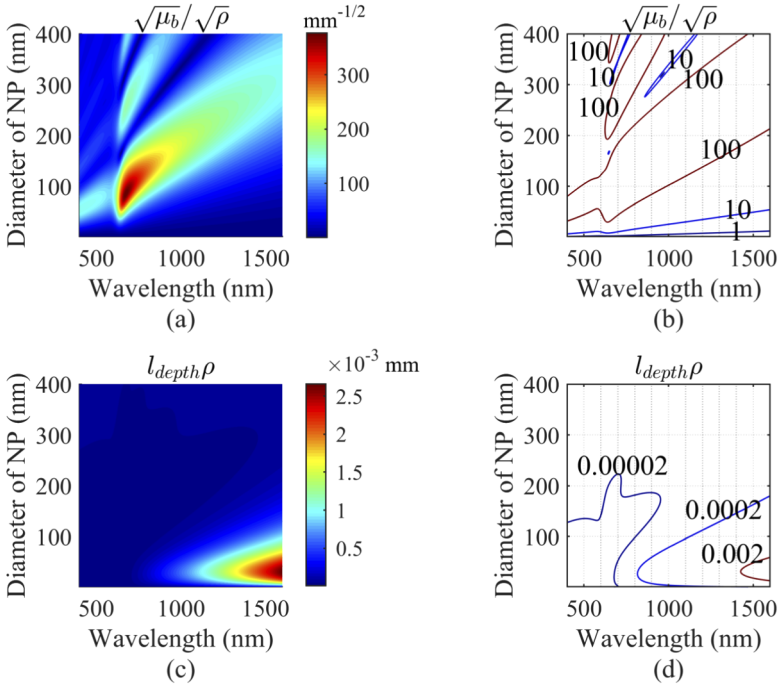

Fig. 5. Backscattering by NPs and penetration depth relative parameter with specific gold NP volume ratio. (a) The backscattering by NPs with volume ratio. (b) Contour map of backscattering by NPs with volume ratio. (c) The penetration depth with volume ratio. (d) Contour map of the penetration depth with volume ratio.

of NP supports more modes [32]. As shown in Fig. 5(a), when the sizes of the NPs increase, multipolar modes are generated. The peak becomes broader and the central wavelength of the peak shows a red shift. Figure 5(b) is the contour map of Fig. 5(a) to show some boundaries, namely 1 mm$^{-1/2}$, 10 mm$^{-1/2}$ and 100 mm$^{-1/2}$. If the penetration depth does not need to be considered, for the same volume ratio of NP suspensions the optimized region appears when in the incident wavelength ranges from about 500 nm to about 1000 nm for a diameter region from about 50 nm to about 200 nm.

If the penetration depth is taken into consideration, the penetration depth multiplied by the volume ratio shown in Fig. 5(c) can be used to restrict the optimized region. If the values shown in Fig. 5(c) are divided by ρ, the penetration depth can be obtained. Figure 5(d), the contour map of Fig. 5(c), shows some boundaries which will be used to evaluate the penetration depth levels. Some specific values are chosen in Fig. 5(d) namely 2×10^{-3} mm, 2×10^{-4} mm and 2×10^{-5} mm. For example, for the same volume ratio 1×10^{-6}, the corresponding penetration depths are 2000 mm, 200 mm and 20 mm respectively. It can be seen from Fig. 5(d) that for NPs' sizes smaller than 200 nm, the penetration depths for the infrared incident light are longer than those in the visible incident light range. For larger size NPs and in the whole wavelength range, the penetration depths are between about 20 mm and about 200 mm if the volume ratio is 1×10^{-6}.

The light wavelength at 1550 nm is what we are mostly concerned with because the light source of the optical system for strain detection (LUNA ODiSI-B) is around this wavelength as well as the light source of the OCT which we will build for the optical fiber interfaces test. In the next part, the optimized light enhancement for gold NPs in fused silica at 1550 nm will be investigated.

Optics EXPRESS

3.2. Optimized light enhancement for gold NPs in fused silica at 1550 nm wavelength

According to Eq. (21), $\sqrt{\mu_b}$ is proportion to $\sqrt{\rho}$. Therefore, in order to determine the maximum value of light enhancement coefficient for a certain diameter of NP, ρ needs to be increased to its maximum within the limitation of the penetration depth. If the maximum of ρ is derived, then the corresponding maximum light enhancement coefficients can be derived. The maximum of ρ and the corresponding maximum light enhancement coefficients for $z = 0$ are shown in Fig. 6.

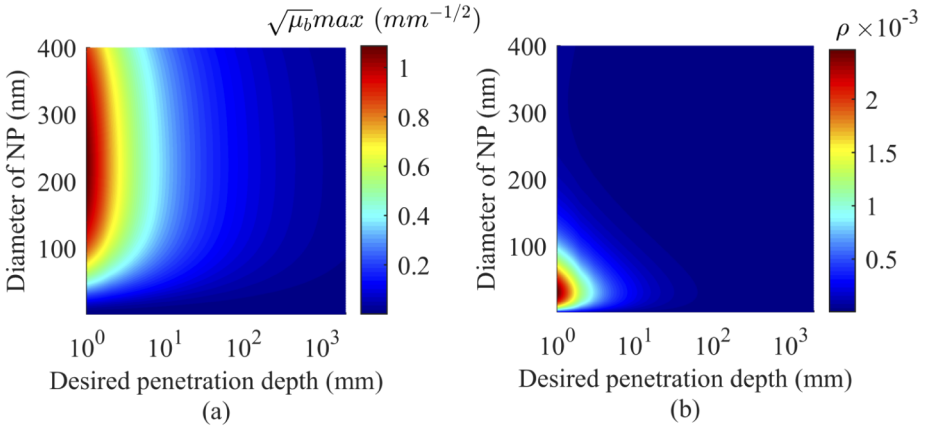

Fig. 6. The maximum $\sqrt{\mu_b}$ with the corresponding volume ratio ρ; the desired penetration depth in the figure is set to be from 1 mm to 2 m; the diameter of the NP is from 1 nm to 400 nm. (a) The maximum $\sqrt{\mu_b}$. (b) The corresponding volume ratio ρ.

For the whole desired penetration depth shown in Fig. 6, from 1 mm to 2 m, the maximum of $\sqrt{\mu_b}$ occurs at the diameter of NPs of about 224 nm as shown in Fig. 6(a). The corresponding volume ratios ρ to achieve the maximums of $\sqrt{\mu_b}$ are shown in Fig. 6(b). It can be seen from Fig. 6(b) that smaller size gold NPs have a lower scattering, for example a NP size below 50 nm even if the volumn ratio is much higher than larger size gold NPs as shown in Fig. 6(a). Another thing to be noted is that the optimized size of gold NPs to achieve the highest scattering is at 224 nm, which is different from the result from Fig. 5(a). In Fig. 5(a), the maximum value is obtained for NPs of about 315 nm at the incident wavelength 1550 nm. It is strange at first glance. One reason for this is that the penetration depth which was defined in order to determine the scattered light in a desired depth does not decrease dramatically and limits the volume ratio. $\sqrt{\mu_b}$ is related to the volume ratio. If we are not concerned about the attenuation caused by the NPs and only look to the higher scattering at the start of the doping fiber, the optimized size of gold NPs is 315 nm.

Figure 7 shows the maximum $\sqrt{\mu_b}$ (maximum $R_{\text{enhancement}}$ at $z = 0$) with the corresponding volume ratio ρ at the optimized NP diameter (224 nm). In the next part, three cases of light enhancement by NPs at the optimized size of NPs (224 nm) with a broadband Gaussian spectra light source with central wavelength 1550 nm will be shown.

3.3. Case of 224 nm diameter gold NPs in fused silica at 1550 nm wavelength

An OCT system whose central wavelength is at 1550 nm and has a FMHW of 60 nm was used to detect the scattered light between the optical fiber end tips. The gold NPs with the optimized size (224 nm diameter) are introduced into the RI matching liquid. The signals detected by the OCT are used to recover the reflected light signals in the optical fiber with the same size and concentration of gold NPs.

Optics EXPRESS

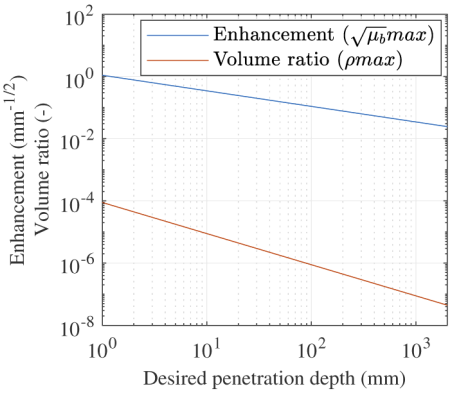

Fig. 7. The maximum $\sqrt{\mu_b}$ with the corresponding volume ratio ρ at the optimized NP diameter (224 nm).

Three cases are simulated. The penetration depths are set at 10 mm, 100 mm and 1000 mm, respectively. The attenuation of the RI matching liquid is assumed as 0.02 mm^{-1}, Γ=1. Other parameters used in the calculations are listed in Tables 2 and 3.

Table 2. Three Cases for Calculation

l_{depth}	ρ_{max}	c	μ_b	μ_{extNP}
10 mm	8.87×10^{-6}	1.51×10^{9} mL^{-1}	1.15×10^{-1} mm^{-1}	6.93×10^{-2} mm^{-1}
100 mm	8.87×10^{-7}	1.51×10^{8} mL^{-1}	1.15×10^{-2} mm^{-1}	6.93×10^{-3} mm^{-1}
1000 mm	8.87×10^{-8}	1.51×10^{7} mL^{-1}	1.15×10^{-3} mm^{-1}	6.93×10^{-4} mm^{-1}

Table 3. Other Parameters Used for Calculation

Parameter	Value
I_0	1 mW
K	1.0 A/W
T_1	1
$2\sigma_0$	4.75 µm
$\Omega \approx \Omega'$	0.0252
$\mu_{Optical\ fiber}$	2.99×10^{-8} mm (0.13 dB/km)
$n_{Optical\ fiber} = n_{liquid}$	1.452

The Monte Carlo Method is used in the calculation to generate the scattered signals detected by the OCT system according to Eqs. (6) and (15) as shown in Fig. 8(a). For each spatial resolution (12 µm), 1000 random points are used for the Monte Carlo calculation. Then, the detected signals by the OCT system are adjusted to the equivalent signals in the optical fiber based on Eq. (16) and then the light intensity signals can be recovered based on Eq. (11).

The recovered signals are shown in Fig. 8(b). The total calculating time is about 13 h on a computer with the 1.80 GHz central processing unit (Intel i7-10610U) for the calculation. Fig. 8(a) shows the results detected by the photodetector in the structure of the optical fiber end tips with the RI matching liquid containing 224 nm size gold NPs. The total depth shown in Fig. 8(a) presents the distance between the two optical fiber end tips in the simulation, but for a real setup the total depth depends on the liquid bubble's size. Figure 8(b) is the corresponding reflected light in the liquid recoupled into optical fiber which is calculated from the generated

Optics EXPRESS

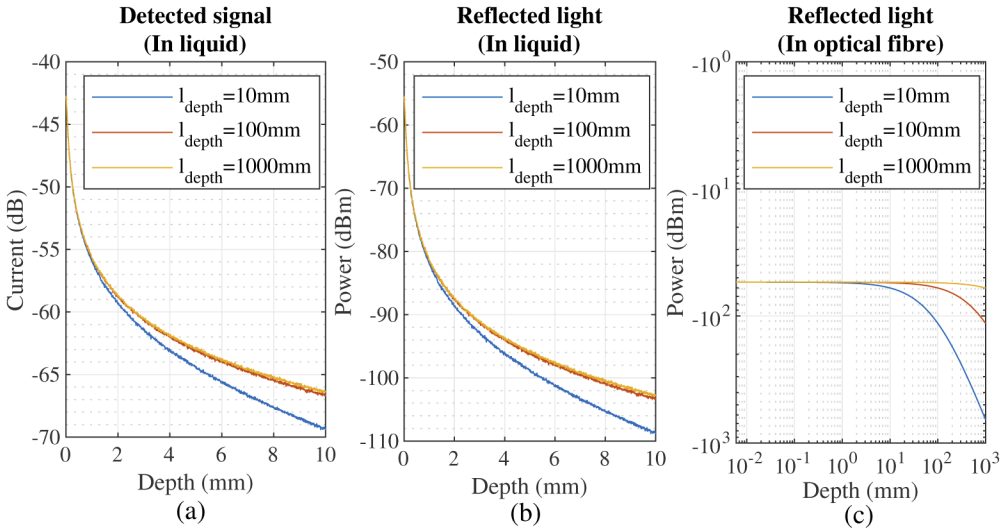

Fig. 8. Detected signal by the OCT system and the recovered signals in the optical fiber. (a) The current from the photodetector of the OCT system simulated between the optical fiber interfaces with RI matching liquid containing gold NPs. (b) The corresponding reflected light in the liquid recoupled into optical fiber. (c) The recovered reflected light power in the optical fiber.

data from Fig. 8(a). It can be seen that there are highly reflected signals from the gold NPs (about −55 dBm) near one end tip of the optical fiber. The corresponding reflected light signal to the incident light is about −36 dB/mm, which is much higher than the reflected to incident light ratio in the optical fiber (about −100 dB/mm [33]). Figure 8(c) shows the recovered reflected light signals in the optical fiber according to the relationship between the detected signals between optical fiber interfaces and in the optical fiber. In Fig. 8(c), the reflected signal at the penetration depths is about 6 dBm lower than at the beginning of the NP-doped optical fiber sensors (the penetration depths are 10 mm, 100 mm and 1000 mm respectively), so the corresponding loss of current is about 3 dBm at its penetration depth.

For the 1550 nm wavelength light source, the attenuation from the optical fiber is low, but for other wavelength regions the attenuation can be high. Therefore, the loss may be much higher than 3 dBm for other regions of wavelengths of the light source. It also needs to be noted that for the case that the wavelenghts of the light source are near the resonance peaks of gold NPs with a broad bandwidth, the approximation may have a large error and the recoupled light should be calculated by Eq. (1).

The optical fiber in this paper is a solid optical fiber. To dope gold NPs in an optical fiber, different sizes of homogeneous gold NPs can be synthesized [34,35] and the shape of the gold NPs can be well controlled [36,37]. The solution doping method [38,39] can then be used to dope gold NPs with porous silica soot by conventional modified chemical vapor deposition (MCVD) process [6,40].

4. Conclusion

The relationship between the two models, the light scattering model at optical fiber interfaces and light scattering model in the optical fiber, has been obtained. The optimized sizes for light scattering enhancement have been obtained by consideration of the penetration depth or without considering the penetration depth. For 1550 nm incident light, the best size of gold NPs for light

Optics EXPRESS

enhancement is around 315 nm if the penetration depth is not taken into consideration. If the penetration depth is taken into consideration the optimized size of gold NPs is about 224 nm. Three cases at the optimized sizes and concentrations are shown with their desired penetration depths to show the distributed reflected signals in the three NP-doped optical fibers. These results can be used for developing highly scattering gold NP-doped optical fiber sensors which rely on high intensity of backscattered light for the future.

Funding. China Scholarship Council (201806020197).

Disclosures. The authors declare no conflicts of interest.

Data availability. The dataset for the results in the paper is available in the 4TU.ResearchData, Ref. [41].

References

1. X. Bao and L. Chen, "Recent progress in distributed fiber optic sensors," Sensors **12**(7), 8601–8639 (2012).
2. R. D. Sante, "Fibre optic sensors for Structural Health Monitoring of aircraft composite structures: Recent advances and applications," Sensors **15**(8), 18666–18713 (2015).
3. P. M. Bueno, M. Martinez, C. Rans, and R. Benedictus, "Strain monitoring using a Rayleigh backscattering system for a composite UAV wing instrumented with an embedded optical fiber," Adv. Mater. Res. **1135**, 1–19 (2016).
4. A. Güemes, A. Fernandez-Lopez, and P. Fernandez, "Damage detection in composite structures from fibre optic distributed strain measurements," in *Proceedings of EWSHM-7th European Workshop on Structural Health Monitoring*, L. Cam, Vincent, Mevel, Laurent, Schoefs, and Franck, eds. (Curran Associates, 2018), pp. 528–535.
5. A. Barrias, J. Casas, and S. Villalba, "A review of distributed optical fiber sensors for civil engineering applications," Sensors **16**(5), 748 (2016).
6. W. Blanc and B. Dussardier, "Formation and applications of nanoparticles in silica optical fibers," J. Opt. **45**(3), 247–254 (2016).
7. C. Molardi, S. Korganbayev, W. Blanc, and D. Tosi, "Characterization of a nanoparticles-doped optical fiber by the use of optical backscatter reflectometry," *Proc. SPIE* 1082121 (2018).
8. A. Beisenova, A. Issatayeva, I. Iordachita, W. Blanc, C. Molardi, and D. Tosi, "Distributed fiber optics 3D shape sensing by means of high scattering NP-doped fibers simultaneous spatial multiplexing," Opt. Express **27**(16), 22074 (2019).
9. P. Bulot, O. Cristini, M. Bouet, A. Demol, L. Bigot, G. Bouwmans, S. Plus, R. Habert, G. Laffont, and M. Douay, "OFDR distributed temperature sensing at 800°C on a fiber with enhanced Rayleigh scattering profile by doping," in *Advanced Photonics*, OSA Technical Digest (online), (Optical Society of America, 2018), p. BM3A.2.
10. C. S. Kim, P. Wilder-Smith, Y. Ahn, L. L. Liaw, Z. Chen, and Y. J. Kwon, "Enhanced detection of early-stage oral cancer in vivo by optical coherence tomography using multimodal delivery of gold nanoparticles," J. Biomed. Opt. **14**(3), 034008 (2009).
11. Y. Huang, M. Li, D. Huang, Q. Qiu, W. Lin, J. Liu, W. Yang, Y. Yao, G. Yan, N. Qu, V. V. Tuchin, S. Fan, G. Liu, Q. Zhao, and X. Chen, "Depth-resolved enhanced spectral-domain OCT imaging of live mammalian embryos using gold nanoparticles as contrast agent," Small **15**(35), 1902346 (2019).
12. E. İ. Altınoğlu and J. H. Adair, "Near infrared imaging with nanoparticles," Wiley Interdiscip. Rev.: Nanomed. Nanobiotechnol. **2**(5), 461–477 (2010).
13. Y. Ponce de León, J. Pichardo-Molina, N. Alcalá Ochoa, and D. Luna-Moreno, "Contrast enhancement of optical coherence tomography images using branched gold nanoparticles," J. Nanomater. **2012**, 1–9 (2012).
14. X. Wang, R. Benedictus, and R. M. Groves, "Modelling of light scattering by gold nanoparticles at optical fibre interfaces," J. Opt. **23**(3), 035602 (2021).
15. D. Huang, E. Swanson, C. Lin, J. Schuman, W. Stinson, W. Chang, M. Hee, T. Flotte, K. Gregory, C. Puliafito, and J. G. Fujimoto, "Optical coherence tomography," Science **254**(5035), 1178–1181 (1991).
16. M. Tanaka, M. Hirano, K. Murashima, H. Obi, R. Yamaguchi, and T. Hasegawa, "1.7- μm spectroscopic spectral-domain optical coherence tomography for imaging lipid distribution within blood vessel," Opt. Express **23**(5), 6645–6655 (2015).
17. P. Liu, R. M. Groves, and R. Benedictus, "3D monitoring of delamination growth in a wind turbine blade composite using optical coherence tomography," NDT & E Int. **64**, 52–58 (2014).
18. A. Quirantes, F. Arroyo, and J. Quirantes-Ros, "Multiple light scattering by spherical particle systems and its dependence on concentration: a T-matrix study," J. Colloid Interface Sci. **240**(1), 78–82 (2001).
19. C. F. Bohren and D. R. Huffman, *Absorption and Scattering of Light by Small Particles* (Wiley, 1998).
20. J. M. Schmitt, A. R. Knuettel, A. H. Gandjbakhche, and R. F. Bonner, "Optical characterization of dense tissues using low-coherence interferometry," *Proc. SPIE* 1889 (1993).
21. J. M. Schmitt, A. Knuttel, M. Yadlowsky, and M. A. Eckhaus, "Optical-coherence tomography of a dense tissue: statistics of attenuation and backscattering," Phys. Med. Biol. **39**(10), 1705–1720 (1994).
22. J. A. Izatt, E. A. Swanson, J. G. Fujimoto, M. R. Hee, and G. M. Owen, "Optical coherence microscopy in scattering media," Opt. Lett. **19**(8), 590–592 (1994).

Optics EXPRESS

23. T. van Leeuwen, D. Faber, and M. Aalders, "Measurement of the axial point spread function in scattering media using single-mode fiber-based optical coherence tomography," IEEE J. Sel. Top. Quantum Electron. **9**(2), 227–233 (2003).
24. J. Xi, Y. Chen, and X. Li, "Characterizing optical properties of nano contrast agents by using cross-referencing OCT imaging," Biomed. Opt. Express **4**(6), 842–851 (2013).
25. L. B. Scaffardi and J. O. Tocho, "Size dependence of refractive index of gold nanoparticles," Nanotechnology **17**(5), 1309–1315 (2006).
26. C. G. Granqvist and O. Hunderi, "Optical properties of ultrafine gold particles," Phys. Rev. B **16**(8), 3513–3534 (1977).
27. P. B. Johnson and R. W. Christy, "Optical constants of the noble metals," Phys. Rev. B **6**(12), 4370–4379 (1972).
28. H. Inouye, K. Tanaka, I. Tanahashi, and K. Hirao, "Ultrafast dynamics of nonequilibrium electrons in a gold nanoparticle system," Phys. Rev. B **57**(18), 11334–11340 (1998).
29. I. H. Malitson, "Interspecimen comparison of the refractive index of fused silica," J. Opt. Soc. Am. **55**(10), 1205–1209 (1965).
30. M. Lines, "Can the minimum attenuation of fused silica be significantly reduced by small compositional variations? I. Alkali metal dopants," J. Non-Cryst. Solids **171**(3), 209–218 (1994).
31. M. Wandel, "Attenuation in silica-based optical fibers," Ph.D. thesis, Tech. Univ. Denmark (2005).
32. T. Liu, R. Xu, P. Yu, Z. Wang, and J. Takahara, "Multipole and multimode engineering in Mie resonance-based metastructures," Nanophotonics **9**(5), 1115–1137 (2020).
33. P. Lu, S. J. Mihailov, D. Coulas, H. Ding, and X. Bao, "Low-loss random fiber gratings made with an fs-IR laser for distributed fiber sensing," J. Lightwave Technol. **37**(18), 4697–4702 (2019).
34. C. Daruich De Souza, B. Ribeiro Nogueira, and M. E. C. Rostelato, "Review of the methodologies used in the synthesis gold nanoparticles by chemical reduction," J. Alloys Compd. **798**, 714–740 (2019).
35. S. Kumar, B. K. Kaushik, R. Singh, N. Chen, Q. S. Yang, X. Zhang, W. Wang, and B. Zhang, "LSPR-based cholesterol biosensor using a tapered optical fiber structure," Biomed. Opt. Express **10**(5), 2150–2160 (2019).
36. G. Frens, "Controlled nucleation for the regulation of the particle size in monodisperse gold suspensions," Nat. Phys. Sci. **241**(105), 20–22 (1973).
37. H. Xia, S. Bai, J. Hartmann, and D. Wang, "Synthesis of monodisperse quasi-spherical gold nanoparticles in water via silver (I)-assisted citrate reduction," Langmuir **26**(5), 3585–3589 (2010).
38. T. Lindstrom, E. Garber, D. Edmonson, T. Hawkins, Y. Chen, G. Turri, M. Bass, and J. Ballato, "Spectral engineering of optical fiber preforms through active nanoparticle doping," Opt. Mater. Express **2**(11), 1520–1528 (2012).
39. C. Kucera, B. Kokuoz, D. Edmondson, D. Griese, M. Miller, A. James, W. Baker, and J. Ballato, "Designer emission spectra through tailored energy transfer in nanoparticle-doped silica preforms," Opt. Lett. **34**(15), 2339–2341 (2009).
40. D. Tosi, C. Molardi, and W. Blanc, "Rayleigh scattering characterization of a low-loss MgO-based nanoparticle-doped optical fiber for distributed sensing," Opt. Laser Technol. **133**, 106523 (2021).
41. X. Wang, "Matlab code and dataset for light scattering by gold NPs in fused silica," 4TU.ResearchData.Dataset (2021), https://doi.org/10.4121/14540823.